submitted APL 3/8/99 1880

Evanescent field imaging of an optical fiber Bragg grating

J.D. Mills, C.W.J. Hillman, and W.S. Brocklesby
Optoelectronics Research Centre, University of Southampton, Southampton, SO17 1BJ, UK

B.H.Blott
Department of Physics and Astronomy, University of Southampton, Southampton, SO17 1BJ, UK

Abstract

We have investigated the evanescent field associated with an optical fiber Bragg grating using the sub-wavelength imaging properties of scanning near-field optical microscopy (SNOM). Imaging of either the field distribution within the grating, or the periodic refractive index changes along the grating can be performed by tuning the launched light on or off the grating resonance. These measurements reveal non-uniformity in the resonant standing-wave pattern that occur due to phase errors in the refractive index profile of the grating under study.

trimmed to the length of the 44mm glass block and further polished on its end faces to ensure that light could be coupled easily into the grating and the mode pattern examined at the output. The grating section of the fiber which had an overall length L=8mm and a refractive index period Λ=570nm was at the midway point along the length of the block. SNOM scanning was performed with an uncoated tapered optical fiber tip, heated and drawn to a 50nm diameter on a Sutter Instrument P2000 micropipette puller. The tip was positioned by piezoelectric actuators and held at a constant 20nm away from the sample surface by use of shear force feedback[10], enabling us to monitor any movement of the probe in the direction normal to the polished surface due to variations in topography. Since the exponentially dependent evanescent field is sensitive to any displacement in this direction, our set-up therefore allowed us to compare optical and topographical data to identify any induced artifacts. Within the experimental set-up a spectrum analyzer was used to monitor the back-reflected light and a photo-diode to measure the intensity of light passing through the grating. The sample had first order resonance at λ_1=1540nm with reflectivity $\mathbf{R_1}$~0.98, although to maximize detection efficiency second order resonance (λ_2=774.8nm, $\mathbf{R_2}$ ~0.60) was employed for much of the investigation. Two types of laser were utilized during the experiment, a 1mW HeNe at 632.8nm and a single frequency tunable diode laser with a range 772.2-788.7nm and maximum power 5mW. Careful alignment of the lasers allowed a single mode condition to be maintained.

The use of SNOM to image the evanescent field associated with an optical waveguide is not a new technique[11]. Often referred to as photon scanning tunneling microscopy (PSTM), the method has already been used to map channel wave-guides[12], Y-branch wave-guides[13], and to observe the Tien effect in wave-guides[14]. When a SNOM tip is brought within the exponentially decaying evanescent field associated with a waveguide, the detected intensity at a given point is expressed by[15]

$$\mathbf{I} = \mathbf{I_0} \exp(-2\mathbf{qz}) + \mathbf{I_s} \qquad (1)$$

where $\mathbf{I_0}$ is the intensity at the surface, $\mathbf{z}$ is the height above the surface, $\mathbf{I_s}$ is the stray scattered light intensity and $\mathbf{q}$ is given by

$$\mathbf{q} = \mathbf{k}(\mathbf{n_e}^2 - 1)^{1/2} \qquad (2)$$

where $\mathbf{k} = 2\pi/\lambda$ and $\mathbf{n_e}$ is the effective refractive index. In the case of our fiber grating, movement in an x-y plane parallel to the polished surface and therefore at constant $\mathbf{z}$ ensured that variables in the above equations were limited to $\mathbf{I_0}$ and $\mathbf{n_e}$.

Figure (1a) shows the results of a 4μm x 4μm scan with 67nm pixel size and the laser tuned to second order resonance. The image is such that the axis of the fiber grating has been positioned down its center. Here the standing wave pattern with fringes of average period Λ/2=285nm can be observed, which produce strong changes in $\mathbf{I_0}$ along the grating. Closer examination reveals that there is non-uniformity in the intensity distribution along the grating due to phase errors resulting from non-uniformity in Λ itself. This becomes clear in Figure (1b), which shows a non-resonant scan in the same position as figure (1a), with λ=784nm. In this figure the electric field intensity $\mathbf{I_0}$ along the grating is constant (no standing wave occurs well off resonance), allowing $\mathbf{n_e}$ to dominate variations in the detected signal. The image now shows the refractive index contrast along the grating, which is clearly not uniform, although the average Λ is indeed 570nm. The ratio of the intensities between bright and dark regions indicate that the variation in the index is of the order 10^{-2}. This estimate confirms the Δn calculated from the known reflectivity and dimensions of the grating. It is expected that index changes of ~10^{-3} could be detected with the present system with even greater resolution being achieved with incident radiation of reduced wavelength. Using the topographical information provided by the SNOM control electronics, we were able to identify clearly several positions on the sample where unevenness in the surface topography of order 20nm caused obvious artifacts in the optical image. None of the structure in the images in figure 1 corresponds to topographical features.

Figure (2) shows a 20μm resonant line scan along the fiber core. The overall envelope of the oscillations is irregular, and does not show the longer-period variation in intensity predicted by grating theory. The inset displays part of the data taken from section 10-14μm on the larger graph along with an identical part of a repeat scan. Allowing for a small (30nm) shift due to thermal drift, the data is reproducible within statistical uncertainty. The similarity between the two scans is typical of the full 20μm. Rather unexpectedly, even scans covering several hundred microns along the axis of this grating reveal no uniform structure. The irregularity is generated by errors in the refractive index profile, which in turn are most likely caused by the generally low spatial coherence of the excimer writing laser itself.

Figure (3a) shows a larger scan off resonance at λ=632.8nm with dimensions 10μm x 10μm and 78nm pixels. The axis of the grating is down the center of the image. The index profile once again has an average period Λ=570nm, demonstrating the independence of these non-resonant images to the wavelength of laser used. Towards the center of this image a faint standing wave can be seen with a wavelength corresponding to 632.8nm/2, formed by reflection off the back face of the glass block.

Scattered light can be observed within the cladding region on either side of the image. Figure (3b) shows a similar scan on second order resonance displaying standing-wave fringes 285nm apart as before. We suggest that this image again demonstrates the effect of phase errors with additional standing waves forming diagonally to the axis of the grating.

In conclusion, we have investigated the evanescent field associated with an optical fiber Bragg grating by using the sub-wavelength imaging properties of scanning near-field optical microscopy (SNOM). We have shown that by launching a laser into the grating and tuning on and off resonance that either the field distribution within the grating or the refractive index contrast along the grating can be imaged. The scans have revealed non-uniformity in the index profile of our particular sample, which in turn has caused phase errors to occur which affect the resonant standing wave distribution. The measurement technique will be significant to the ongoing development of optical fiber Bragg gratings used throughout the telecommunications industry.

Figure Captions

FIG 1: Fiber grating evanescent field images (a) on resonance (774.8nm) showing the standing wave field distribution and (b) off resonance (784nm) where the field distribution along the length of the grating has become flat enough to allow the refractive index profile to dominate. The axis of the grating is down the center of the image in each case.

FIG 2: Repeat, evanescent field resonant line scans along the axis of the fiber grating. Whilst the 20μm scan demonstrates the irregularity of the overall envelope, the inset shows a section of both traces, demonstrating the reproducibility of the measurement.

FIG 3: Fiber grating evanescent field images (a) off resonance (632.8nm) revealing the refractive index contrast and (b) on resonance (774.8nm) displaying the standing wave distribution

[1] G. Meltz, W. W. Morey, W. H. Glenn, Optics Letters **14**, 823 (1989).

[2] K.O. Hill, B. Malo, F. Bilodeau, D.C. Johnson, J. Albert, Appl. Phys. Lett. **62**, 1035-1037, (1993)

[3] W. H. Loh, R. I. Laming, X. Gu, M.N. Zervas, M.J. Cole, T. Widdowson, A.D. Ellis, Electronics Letters **31**, 2203 (1995).

[4] F. Bakhti, P. Sansonetti, C. Sinet, L. Gasca, L. Martineau, S. Lacroix, X. Daxhelet, F. Gonthier, Electronics Letters **33**, 803 (1997).

[5] T. Erdogan, Journal of Lightwave Technology, **15** (8), 1277 (1997).

[6] M.A. Muriel, A. Carballar, J. Azana, IEEE Journal of Quantum Electronics, **35** (4), 548-558 (1999).

[7] B. Malo, D.C. Johnson, F. Bilodeau, J. Albert, K.O. Hill, Opt. Lett. **18** (15), 1277 (1993).

[8] P. E. Dyer, R. J. Farley, R. Giedl, Optics Communications, **115**, 327-334 (1995).

[9] S. T. Huntington, K. A. Nugent, A. Roberts, J. Appl. Phys. **82** (2), 510 (1997).

[10] K. Karrai, R.D. Grober, Appl. Phys. Lett. **66**, 1842 (1995).

[11] H.E. Jackson, J.T. Boyd, Optical and Quantum Electronics **23**, S901 (1991).

[12] A.G. Choo, M.H. Chudgar, H.E. Jackson, G.N. De Brabander, M. Kumar, J.T. Boyd, Ultramicroscopy **57**, 124 (1995).

[13] Y. Toda, M. Ohtsu, Photonics Technology Letters **7**, 84 (1995).

[14] S. Bourzeix, J.M. Moison, F. Mignard, F. Barthe, A.C. Boccara, C. Licoppe, B. Mersali, M. Allovon, A. Bruno, Appl. Phys. Lett. **73**, 1035 (1998).

[15] D.P. Tsai, H.E. Jackson, R.C. Reddick, S.H. Sharp, R.J. Warmack, Appl. Phys. Lett. **56**, 1515 (1990).

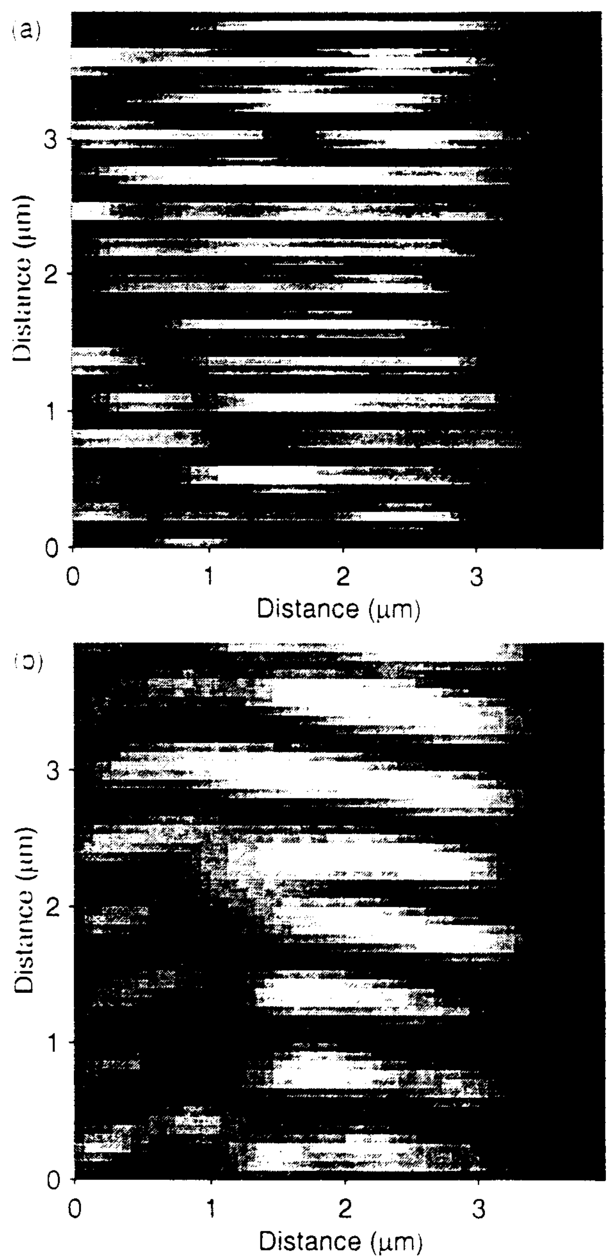
(a)
Distance (μm)
Distance (μm)
(b)
Distance (μm)
Distance (μm)

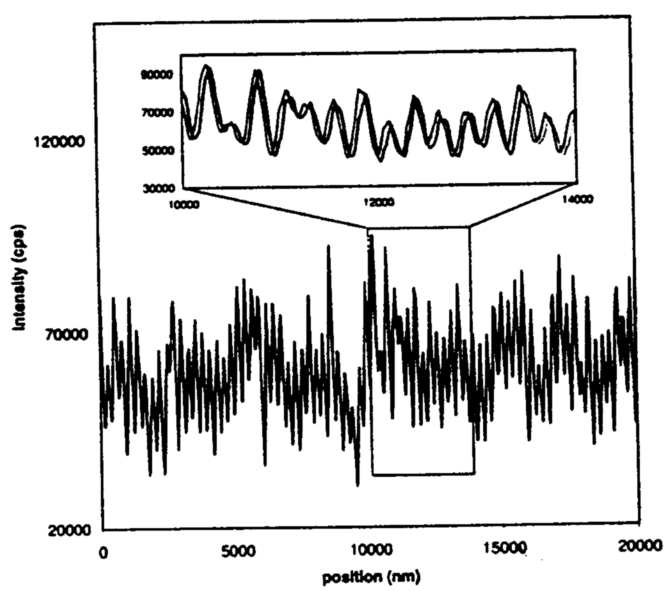

90000
70000
50000
30000
10000
12000
14000
120000
70000
20000
Intensity (cps)
0
5000
10000
15000
20000
position (nm)

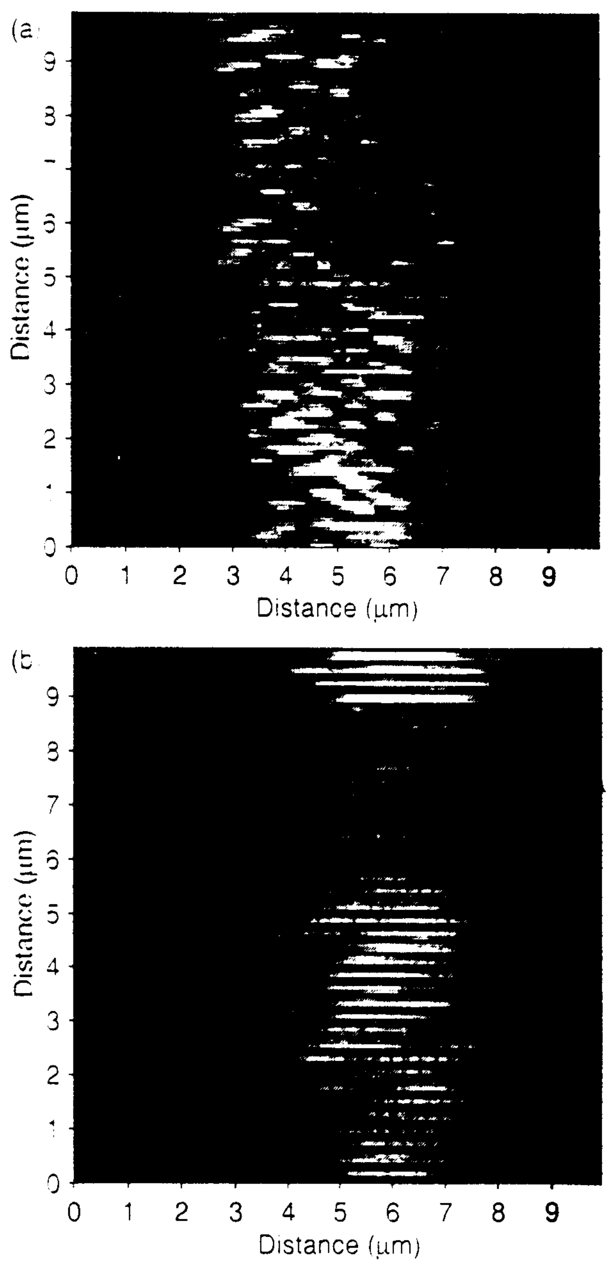
(a)
Distance (μm)
0 1 2 3 4 5 6 7 8 9
Distance (μm)
(b)
Distance (μm)
0 1 2 3 4 5 6 7 8 9
Distance (μm)